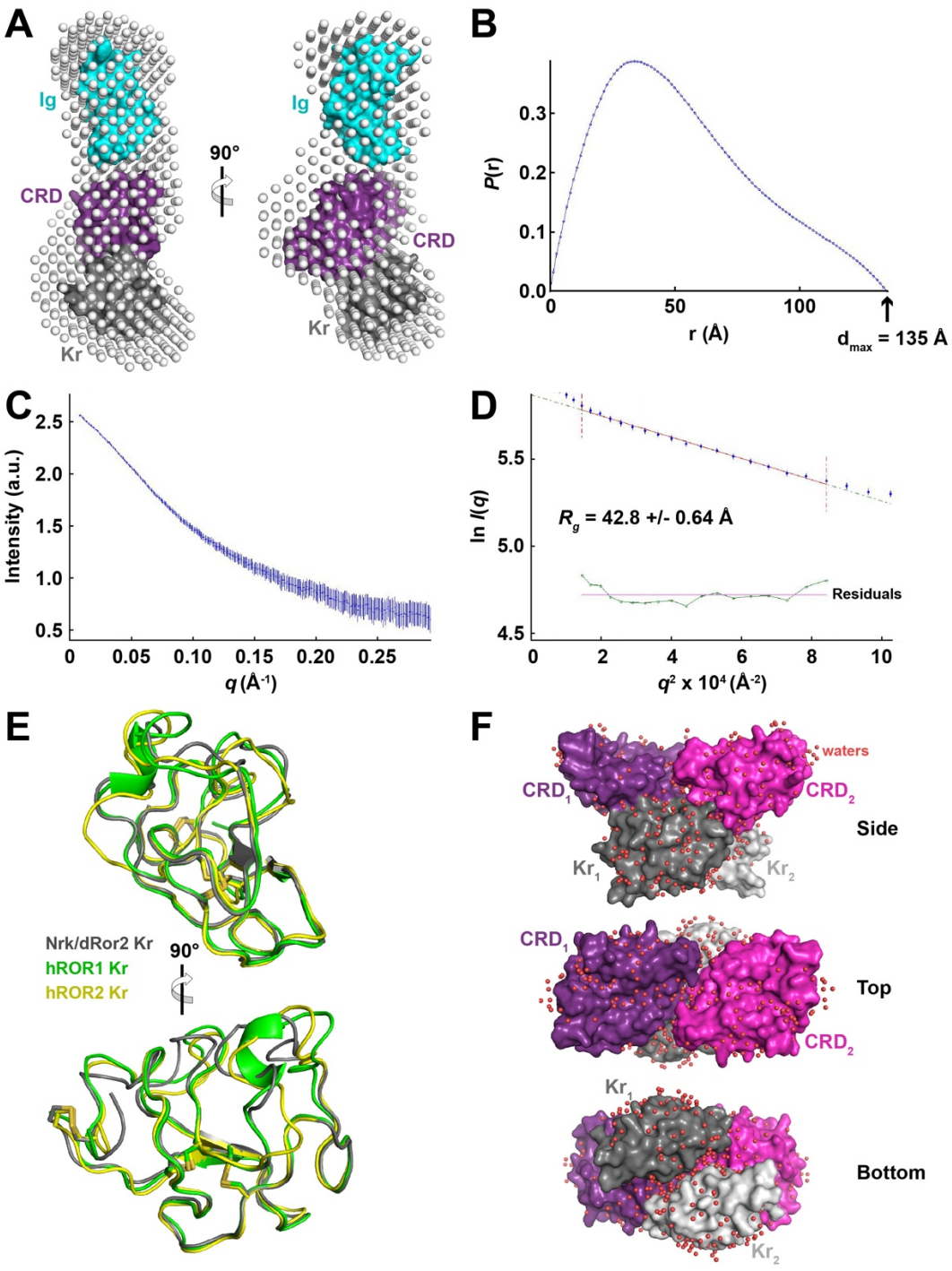

FIGURE S1 – Related to Figure 1

Structural features of ROR family ECRs

(**A**) SAXS-derived most probable molecular envelope for the human ROR2 ECR (see Method Details). The envelope is shown as a collection of spheres from the DAMAVER output, in two orthogonal views. Into the envelope are docked the sNrk structure shown in Figure 1C (CRD plus Kr domain) plus an immunoglobulin (Ig) domain (cyan). This analysis suggests that the Ig extends the ECR as a rod compared with sNrk.

(**B**). Pair distance distribution function or *P*(r) curve for s-hROR2 determined as described in Method Details. The maximum dimension (d_{max}) of s-hROR2 is 135 Å, compared with an estimated 60-65 Å for sNrk and ~45Å for the long axis of an Ig domain.

(**C**) Representative corrected scattering curve for s-hROR2 at 11.3 mg/ml (270 μM) in 25 mM MES, 150 mM NaCl, pH 6.0, with exposure time of 4 s, plotting intensity (*I*) plotted against *q* ($4\pi\sin\theta/\lambda$, where 2*q* is the scattering angle).

(**D**) Guinier analysis of the sample shown in **C**, with the Guinier region ($q^*R_g < 1.3$) marked and residuals of the fit (lower points) shown.

(**E**) Overlay of the Nrk/dRor2 Kringle domain with those determined by X-ray crystallography for hROR1 (green; PDBID: 6BAN) and hROR2 (yellow; PDBID: 6OSH) in complex with potential therapeutic antibodies (Goydel et al., 2020; Qi et al., 2018). Two orthogonal views are shown, as marked.

(**F**) Illustration of the only dimer in the sNrk crystals that buries more than 400 $Å^2$ of surface. Three orthogonal views are shown. One molecule is colored as in Figure 1C, and the other pink (CRD) and white (Kr). Water molecules are shown as red spheres. As can be seen in the top and bottom views, there is clear space between both the CRDs and the Kr domains in this dimer, with water between the molecules. Thus, there is no intimate dimer interface – consistent with the fact that sNrk showed no evidence for dimerization by size exclusion chromatography, SAXS, or analytical ultracentrifugation.

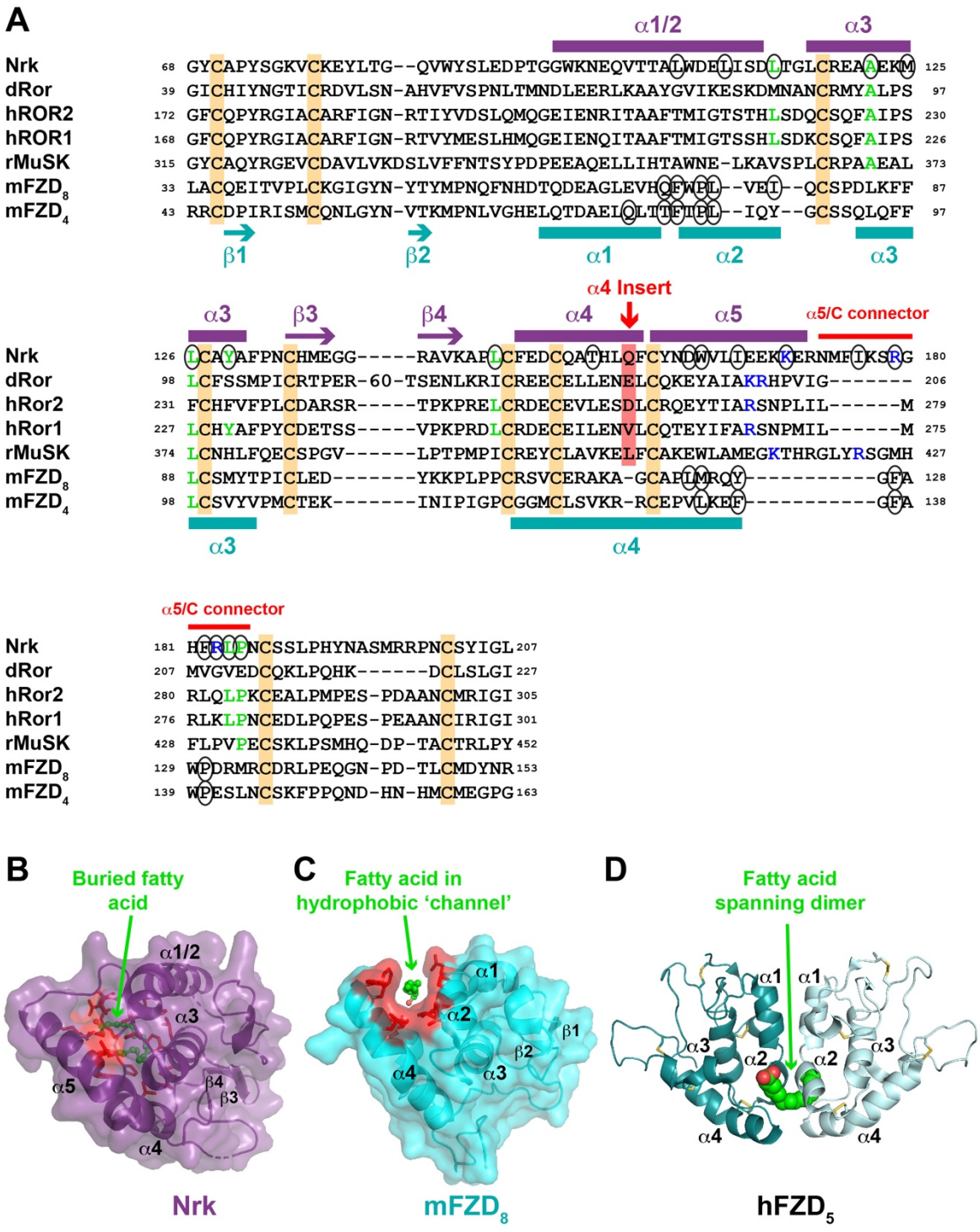

FIGURE S2 – Related to Figure 2.

Sequence comparison of ROR family CRDs

(**A**) Structure-based sequence alignment of *Drosophila* ROR family CRDs with those from human RORs, MuSK, and murine FZDs 4 and 8. Cysteines are shaded yellow/orange. Secondary structure elements are marked on the sequence for Nrk (purple) and mFZD$_8$ (cyan), using the designation introduced by the Leahy lab (Dann et al., 2001). Residues circled in black

contact the bound fatty acid in the Nrk, $mFZD_8$ (Hirai et al., 2019; Janda et al., 2012) and $mFZD_4$ CRD (DeBruine et al., 2017) structures. Those involved in fatty acid binding to the Nrk CRD that are conserved in other CRDs are colored green – noting that hROR1 and hROR2 conserve many of these residues. Basic residues in the α5/C-tail connector that 'clamp' the fatty acid headgroup in Nrk's CRD are conserved (albeit not precisely) in location in all other ROR CRDs (and MuSK) – and are colored blue – suggesting that all ROR CRDs are capable of the fatty acid binding mode seen for Nrk.. These residues are absent in FZD CRDs, which have a much shorter connection between helix α4 and the C-terminal region. The 'α4 insert' that breaks α4 (and creates α5) is marked with a red arrow.

(**B**) View of the Nrk CRD with transparent surface. Fatty acid-contacting residues are colored red (side-chains shown as sticks) – showing that they form an internal binding site for the buried fatty acid.

(**C**) View of the $mFZD_8$ CRD in the same orientation used for Nrk in **B**. A transparent surface is shown. The fatty acid-contacting residues, many of which are common to $mFZD_8$ and Nrk are colored red (side-chains shown as sticks) and form a prominent hydrophobic 'channel' on the domain's surface – in which the fatty acid resides.

(**D**) Cartoon representation of the $hFZD_5$ CRD dimer structure (PDBID: 5URY), mediated by α1, α2, and α4 and a single fatty acid molecule that lies simultaneously in the hydrophobic channels of both CRDs (Nile et al., 2017).

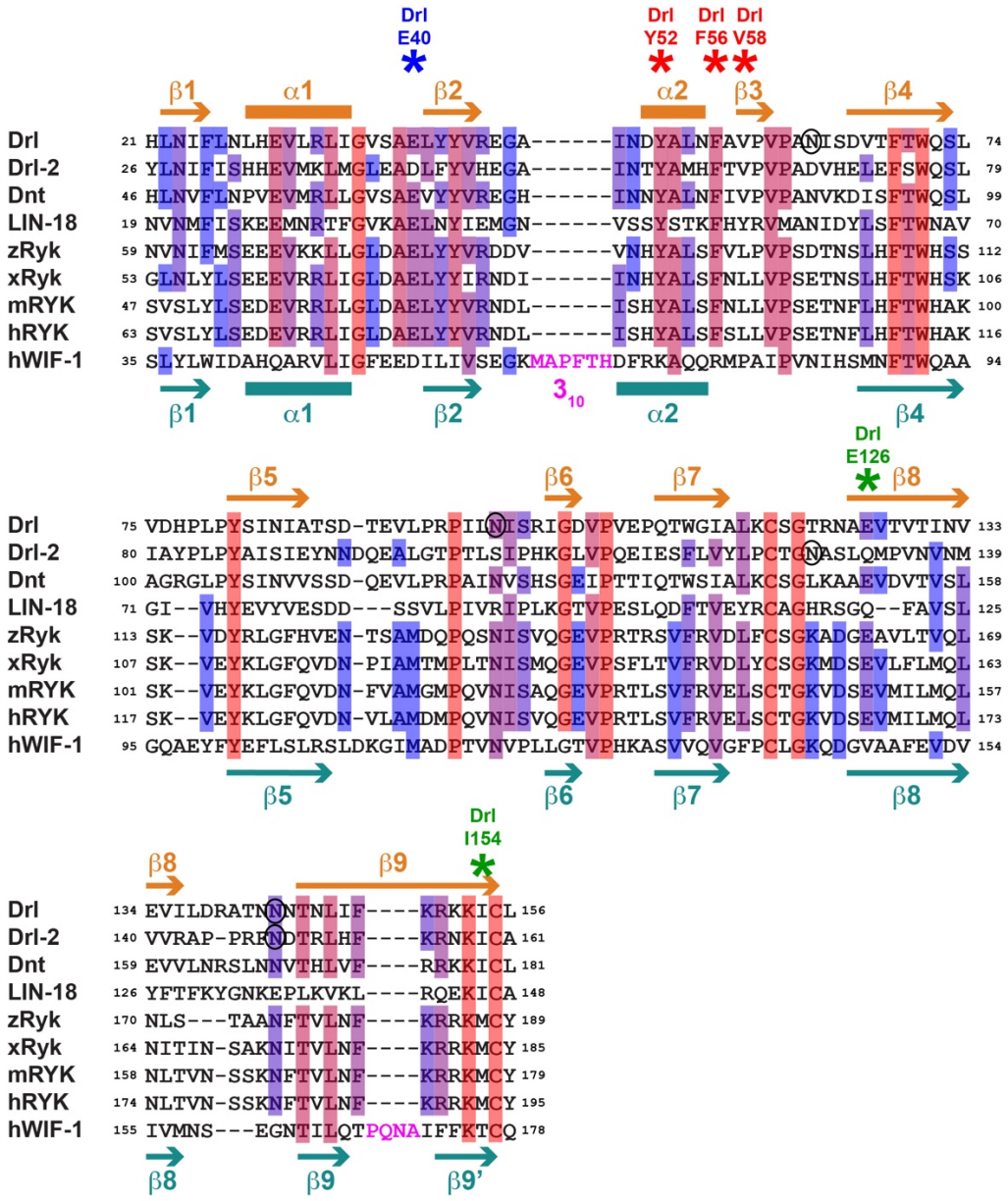

FIGURE S3 – Related to Figure 3.

Sequence comparison of WIF domains

The WIF domains from *Drosophila* RYK/Drl family members are aligned with those of RYK orthologs from *Caenorhabditis elegans* (LIN-18), zebrafish (zRyk), *Xenopus laevis* (xRyk), mouse (mRYK), and human (hRYK), plus the human WIF-1 WIF domain. Alignments are guided by the structures of the sDrl-2 and WIF-1 WIF domains, for which secondary structure elements are shown at the top (in orange) and bottom (deep teal). Sequence conservation is colored from red (conserved in all 9 sequence) to blue (conserved in 5 of 9), revealing key areas of conservation. The inserted 3_{10} helix sequence (MAPFTH) adjacent to α2 is colored magenta, as is the proline-containing insert in β9 (PQNA). Glycosylation sites are circled in black, and residues mutated in sDrl for binding studies are marked with asterisks, colored according to whether they greatly disrupted binding (red), partly disrupted binding (blue), or had no effect (green).

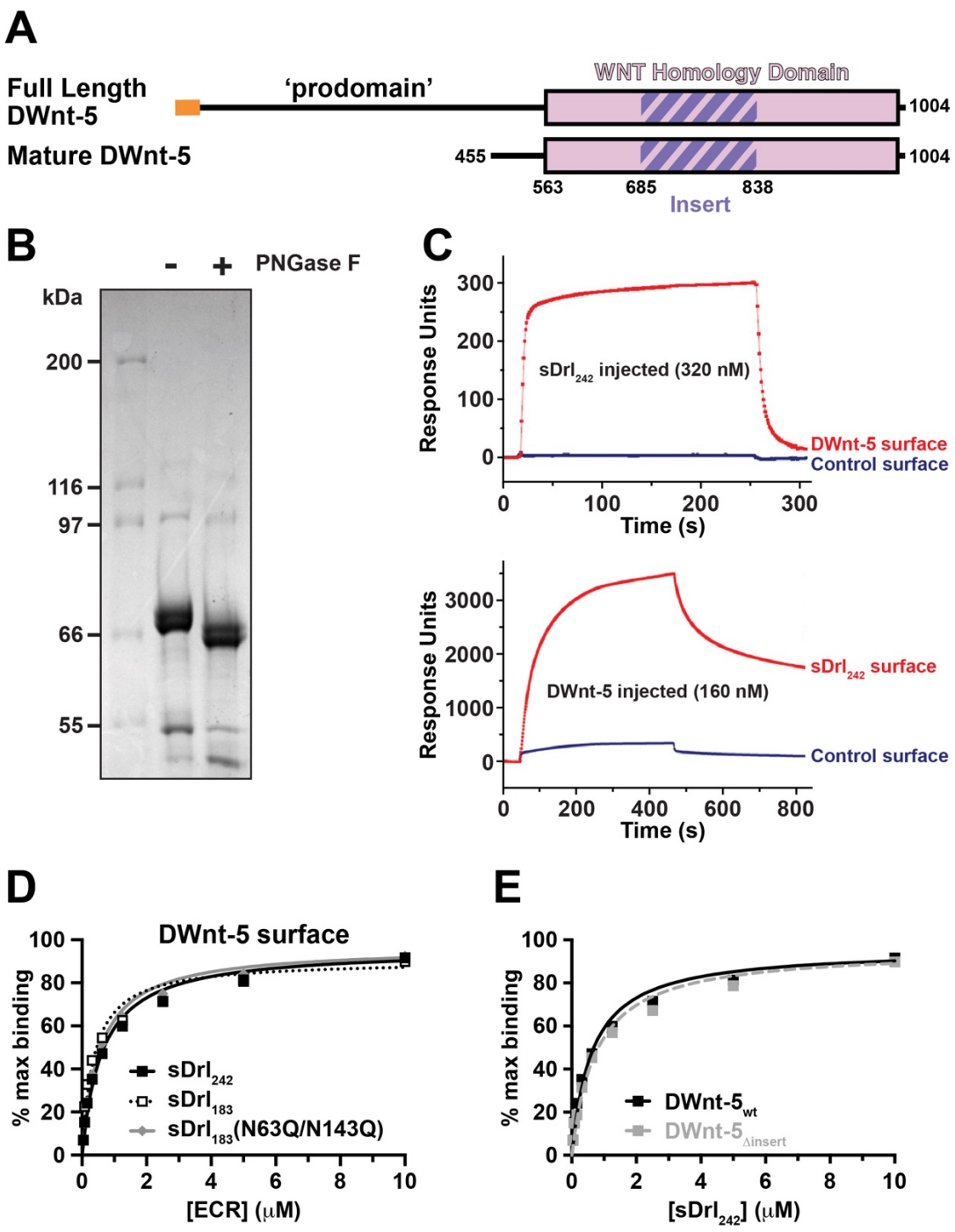

FIGURE S4 – Related to Figure 4.

Characteristics and interactions of DWnt-5

(**A**) Schematic of the DWnt-5 protein. Following the amino-terminal signal sequence (orange) is a long 'prodomain' that was found to be cleaved off when the protein is expressed in an imaginal disc cell line (Fradkin et al., 1995) to yield a mature secreted form of ~80 kDa. As described in the text, the mature protein produced here in S2 cells begins at residue 455 (based on N-terminal sequencing). The protein also has a characteristic insert in its WNT homologous region, from 685 to 838, which does not appear to be involved in RTK binding.

(**B**) Coomassie-stained SDS-PAGE of purified DWnt-5 before and after treatment with PNGase F, showing that it is glycosylated, and the protein core is ~64 kDa.

(**C**) Representative sensorgrams from single SPR experiments (each data point on each binding curve elsewhere represents a single such sensorgram). In the upper panel, 320 nM $sDrl_{242}$ was injected on a sensorchip onto which DWnt-5 had been immobilized. In the lower panel, 160 nM DWnt-5 was instead injected on a sensorchip onto which $sDrl_{242}$ had been immobilized. Note that the signal comes back down to baseline when the DWnt-5 surface was used (upper), but not when the Drl ECR was immobilized (lower), suggesting aggregation of DWnt-5 on the sensorchip surface, and necessitating the regeneration step described in Method Details.

(**D**) Representative SPR binding curves for binding of the complete sDrl ECR ($sDrl_{242}$) and the WIF domain ($sDrl_{183}$) to immobilized DWnt-5, showing no difference. Similarly, mutation of two glycosylation sites (necessary for protein behavior for HDX-MS analysis) had no influence on DWnt-5 binding. Data are representative of at least 2 biological replicates.

(**E**) SPR binding curves comparing binding of $sDrl_{242}$ to immobilized mature DWnt-5 and DWnt-5 from which the 'insert' in **A** had been removed as described in Method Details ($DWnt\text{-}5_{\Delta insert}$). Loss of the insert has no detectable influence on binding. Data are representative of at least 2 biological replicates.

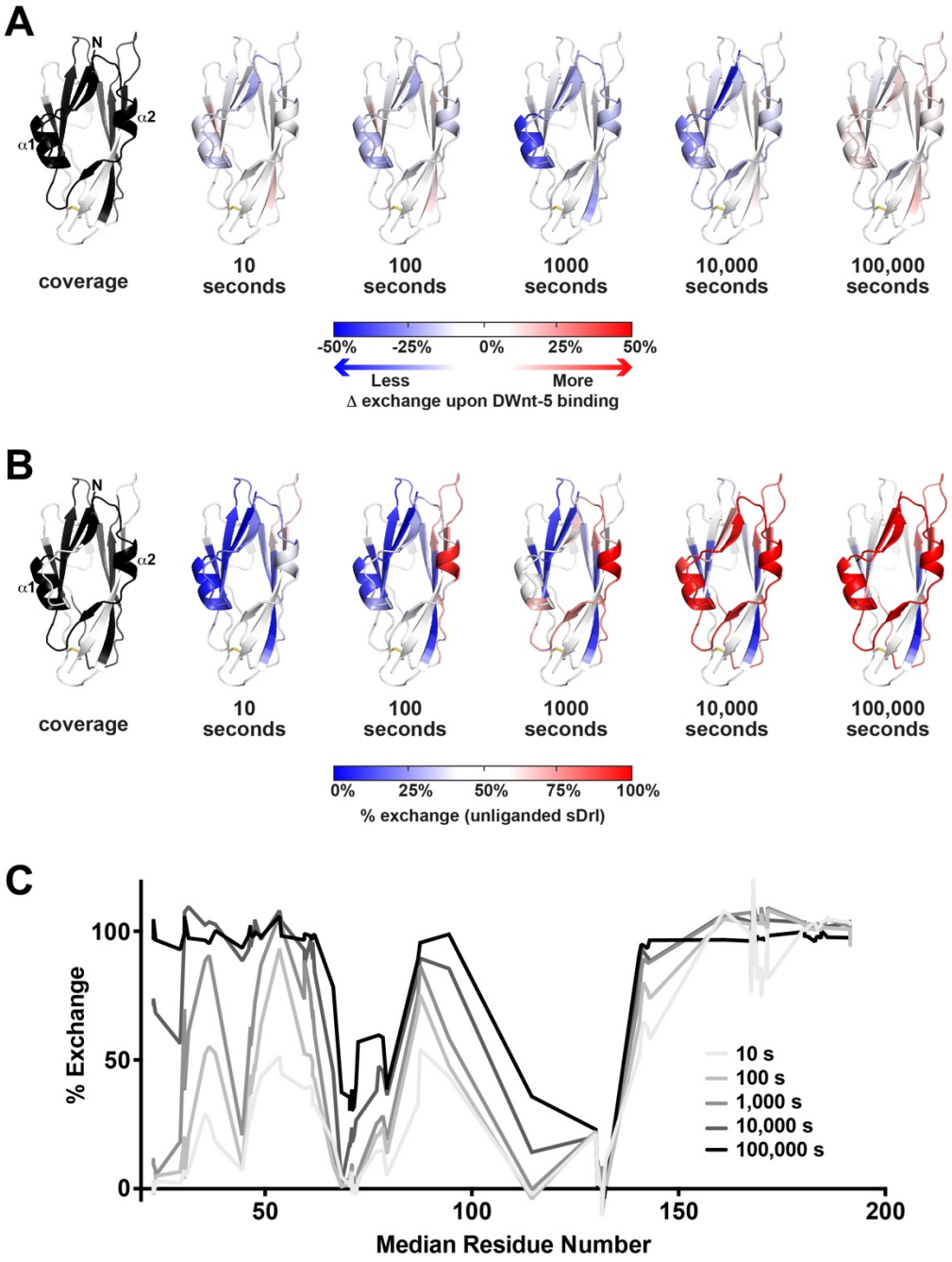

FIGURE S5 – Related to Figure 5.

HDX-MS analysis of sDrl binding to DWnt-5

(**A**) Summary of HDX differences observed in $sDrl_{242}$ in the presence of DWnt-5 protein at ~25 μM (> 10 times K_D, to achieve saturation) as described in Method Details. The left-hand representation of the structure depicts coverage (black regions were detected), which was ~75% of the WIF domain in HDX experiments. Missing peptides were in disulfide bonded regions. For the peptides seen, the percent exchange at the different time-points shown, as a result of DWnt-5 binding is colored according to the scale and mapped onto the structural model. Data for the 1,000 s time-point are shown in Figure 5D.

(**B**) Representation of HDX in unliganded $sDrl_{242}$ across 5 different time points, showing that the regions surrounding the splayed corner of the sandwich (including α1 and α2) are among the most highly exchanging.

(**C**) Plot of exchange data for the 5 time points, with the x axis representing the median residue number of the peptide for which mean exchange is plotted as described (Sheetz et al., 2020).

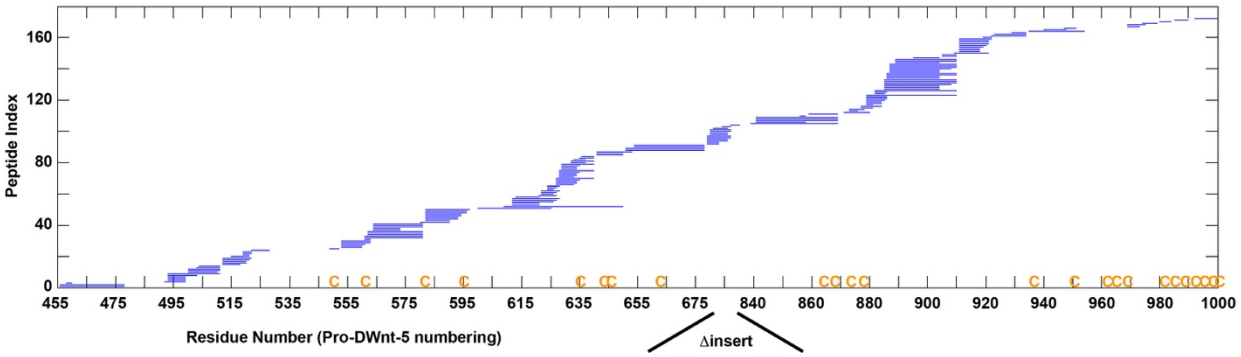

FIGURE S6 – Related to STAR Methods.

Coverage of DWnt-5

Peptide map showing the best coverage obtained for DWnt-$5_{\Delta insert}$ in HDX-MS studies, corresponding to 172 peptides (124 unique peptides). The positions of the 24 cysteines (all in disulfide bonds) in DWnt-$5_{\Delta insert}$ are marked at the bottom in gold text. Sequence numbers correspond to the DWnt-5 sequence in Uniprot (P28466). Note that coverage is very poor in the C-terminal part of the protein – across the entire C-terminal domain of the WNT protein, where there are 12 cysteines.